

## CFD simulation of pervaporation of organic aqueous mixture through silicalite nanopore zeolite membrane

Mansoor Kazemimoghadam<sup>1,\*</sup>, Zahra Amiri-Rigi<sup>2</sup>

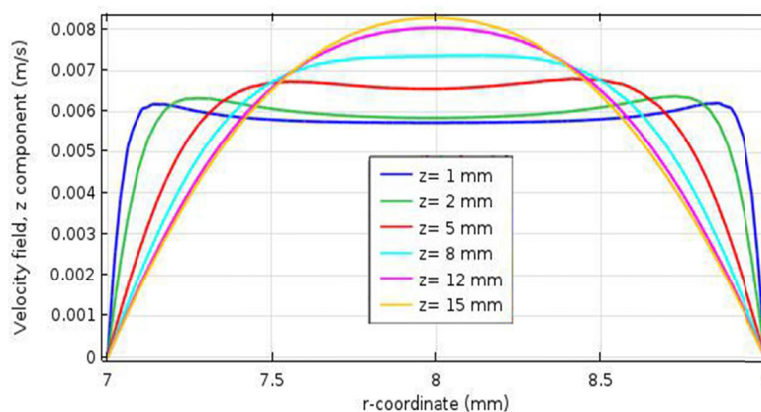
<sup>1</sup> Department of Chemical Engineering, Malek-Ashtar University of Technology, Tehran, Iran

<sup>2</sup> Department of Chemical Engineering, South Tehran Branch, Islamic Azad University, Tehran, Iran

### HIGHLIGHTS

- Silicalite nanopore zeolite membranes were synthesized by in-situ liquid phase hydrothermal method and studied by XRD and SEM techniques.
- Pervaporation tests were carried out for evaluation of the performance of the membranes in the separation of water-UDMH mixtures.
- A comprehensive steady state model was developed for CFD simulation of pervaporation using the finite element method.

### GRAPHICAL ABSTRACT



### ARTICLE INFO

#### Article history:

Received 29 May 2017

Revised 7 August 2017

Accepted 3 October 2017

#### Keywords:

Silicalite

Zeolite membrane

Pervaporation

Water-UDMH separation

CFD simulation

### ABSTRACT

Nanopore silicalite type membranes were prepared on the outer surface of a porous-mullite tube by in situ liquid phase hydrothermal synthesis. The hydrothermal crystallization was carried out under an autogenously pressure, at a static condition and temperature of 180 °C with tetrapropylammonium bromide (TPABr) as a template agent. The molar composition of the starting gel of silicalite zeolite membrane was:  $\text{Na}_2\text{O}/\text{SiO}_2=0.287-0.450$ ,  $\text{H}_2\text{O}/\text{SiO}_2=8-15$ ,  $\text{TPABr}/\text{SiO}_2=0.01-0.04$ . The zeolites calcinations were carried out in air at 530°C, to burn off the template (TPABr) within the zeolites. X-ray diffraction (XRD) patterns of the membranes consisted of peaks corresponding to the support and zeolite. The crystal species were characterized by XRD, and morphology of the supports subjected to crystallization was characterized by scanning electron microscopy (SEM). Performance of silicalite nanoporous membranes was studied for separation of water-unsymmetrical dimethylhydrazine (UDMH) mixtures using pervaporation (PV). Finally, a comprehensive steady state model was developed for the pervaporation of a water-UDMH mixture by COMSOL Multiphysics software version 5.2. The developed model was strongly capable of predicting the effect of various dimensional factors on concentration and velocity distribution within the membrane module. The best silicalite zeolite membranes had a water flux of 3.34 kg/m<sup>2</sup>.h at 27 °C. The best PV selectivity for silicalite membranes obtained was 53.

\* Corresponding author: Tel.: +9821-73203086 ; Fax: +9821-73203080 ; E-mail address: mzkazemi@gmail.com

## 1. Introduction

Unsymmetrical dimethylhydrazine (UDMH) is an organic derivative of hydrazine which is usually used as a propellant. This hazardous material has many other new applications and is widely applied as an oxygen scavenger for boiler-feed water, a starting material for drug and dye intermediates, a catalyst for polymerization reactions, etc. UDMH is very corrosive and its vapor is extremely toxic and carcinogenic [1-3]. Removal of highly hazardous UDMH from water is important for the recovery of valuable organic products, for the recycling of process water and for the treatment of waste water [4]. Generally, traditional azeotropic distillation or extraction can be used to separate organic compounds from their aqueous solutions. However, for low organic concentrations or thermally sensitive organic compounds, distillation is very expensive and also extremely dangerous due to the explosive nature of UDMH.

There has been a growing interest in membrane-based PV technology due to the extreme effectiveness as well as mild operating conditions of this separation technique. Since only a fraction of the solution to be removed is vaporized, the energy consumption will be decreased significantly. Moreover, compared to conventional distillation, PV is a simple technique because only a pump is required to maintain the driving force.

At present, dehydration of organic solvents is the major market of PV. High separation factors and water permeate fluxes are reported in previous studies on pervaporation dehydration of isopropanol, ethanol, n-butanol, n-butyl-acetate, ethylene glycol and acetic acid aqueous solution [5-8]. Uragami *et al.* investigated the effect of immersion time in  $\text{CaCl}_2$  or  $\text{MgCl}_2$  methanol solutions on the permeation flux and separation factor of pervaporation dehydration of ethanol aqueous solution using Alg-DNA/ $\text{Mg}^{2+}$  membrane [9]. Their results showed that after immersing the membrane in methanol solutions, the separation factor increased remarkably for the first 12 hours, after which it started to fall [9].

Zeolite membranes are usually used in pervaporation processes due to their strong potential. These membranes are synthesized using various methods such as hydrothermal in-situ crystallization, chemical vapor phase technique and spray seed coating. Zeolite NaA membranes were reported to be excellent materials for

solvent dehydration by PV [10]. But under slightly severe conditions and under hydrothermal stresses, zeolite NaA membranes behaved unsuitably due to hydrolysis. There have been only a few attempts to develop hydrophilic highly siliceous zeolite membranes of different Si/Al ratios with improved hydrothermal stabilities.

In PV, the feed mixture is contacted with a nonporous perm selective membrane. In general, separation is explained by the steps of sorption into, diffusion through and desorption from the membrane. The latter is usually considered to be fast and taking place at equilibrium, while diffusion is kinetically controlled and the slowest step of the process. Permeation is dependent on sorption and diffusion steps. The driving force for the filtration is created by maintaining a pressure lower than the saturation pressure on the permeate side of the membrane. The mechanism of separation is usually explained in terms of sorption-diffusion processes [11-13].

Many studies have been conducted to model concentration distribution within the membrane module in order to commercialize PV separation systems. There are two major approaches to PV simulations: Molecular Dynamic (MD) simulation and Computational Fluid Dynamic (CFD) simulation. Based on MD, Huang *et al.* developed a model to explain free-volume form and the flexibility and stiffness of polymer chain. Their results, obtained from MD simulations, were in good harmony with the chemical structure of the polyelectrolyte complex membranes (PECMs) [14]. Jain *et al.* (2017) proposed a mathematical model for the purification of n-heptane/thiophene model gasoline using a tubular pervaporation membrane module [15]. Their findings showed that the dimensional factors had positive effects on separation performance of pervaporation membranes.

Based on CFD simulation, Moulik *et al.* developed a steady state model to predict concentration distribution within the membrane module in pervaporation of acetic acid solution [16]. Their results were in good agreement with experimental data, but their model was not perfect, since they didn't model the concentration distribution within the feed section, which significantly affects the concentration profile on the membrane side. Prasad *et al.* also developed a 2D steady state model using the CFD technique [17]. They also modeled the membrane section only and assumed the conditions to be steady state.

As understood, a comprehensive model is required, capable of predicting concentration distribution within

both membrane and feed sub-domains. In this paper, preparation methods of the nanopore silicalite-1 zeolite membrane on mullite support are reported. Performances of the membranes prepared by hydrothermal in situ crystallization were studied in separation of the water-UDMH by PV. Finally, a comprehensive steady state 2D model was proposed based on solving Navier-Stokes equations of mass and momentum transfer, simultaneously. The conservation equations were solved using COMSOL Multiphysics software version 5.2. COMSOL applies the Finite Element Method (FEM) to solve the equations numerically. Effect of various membrane dimensions and feed flow rates was investigated to find the optimum operating conditions. The model obtained here was masterfully capable of predicting concentration distribution of water through both membrane and feed sides of the separation module. The results indicated that the effect of dimensional factors related to the membrane module geometry on concentration distribution is very important and cannot be neglected.

## 2. Experimental

### 2.1. Support preparation

In ceramic membranes, thin dense layers are usually deposited over porous supports. The porous supports provide mechanical strength for the thin selective layers. Porous supports can be made from alumina, cordierite, mullite, silica, spinel, zirconia, other refractory oxides and various oxide mixtures, carbon, sintered metals and silicon carbide.

In this research, mullite supports were prepared from kaolin clay. Kaolin is thermally converted to mullite via high temperature calcinations. The reaction takes place when kaolin is utilized as the sole source of silica and alumina. The reaction can be represented by the following equation:



Free silica ( $4\text{SiO}_2$ ) is generated as a result of this conversion. Free silica was leached out and then porous mullite bodies were prepared. Mullite has several distinct advantages over other materials. Since kaolin is heated to high temperatures to achieve the mullite conversion reaction, strong inter-crystalline bonds

between mullite crystals are formed and this will result in excellent strength and attrition. Leaching time depends on several factors including:

- 1) the quantity of free silica to be removed,
- 2) the porosity of body prior to leaching,
- 3) the concentration of leaching solution, and
- 4) temperature.

Kaolin (SL-KAD grade) was supplied by WBB cooperation, England. Analysis of the kaolin is listed in Table 1. Cylindrical shaped (tubular) bodies were conveniently made by extruding a mixture of about 75-67% kaolin and 25-33% distilled water. Suitable calcination temperatures and periods are those at which kaolin converts to mullite and free silica. Good results were achieved by calcining for about 3 h at temperatures of about 1250 °C [18].

**Table 1.** Analysis of kaolin clay.

Component	Percent (%)	Phases	Percent (%)
SiO <sub>2</sub>	51.9	Kaolinite	79
TiO <sub>2</sub>	0.1	Illite	8
Al <sub>2</sub> O <sub>3</sub>	34.1	Quartz	10
Fe <sub>2</sub> O <sub>3</sub>	1.4	Feldspar	3
K <sub>2</sub> O	0.8	Total	100
Na <sub>2</sub> O	0.1		
L.O.I	11.6		
Total	100		

Free silica was removed from the calcined bodies after leaching by strong alkali solutions. Removal of the silica causes mesoporous tubular supports with very high porosity to be made. Free silica removal was carried out using aqueous solutions containing 20% by weight NaOH at a temperature of 80 °C for 5 h. Supports were rinsed using a lot of hot distilled water for a long time in order to remove all remaining NaOH. Porosity of the supports before leaching was 24.3%, while after treatment it increased to 49%. Flux of the supports before and after free silica removal at 1 bar and 20 °C were 6 and 10 kg/m<sup>2</sup>h, respectively. Porosity of the supports was measured by the water absorption method. Inner and outer diameters and length of the support were 10, 14 and 100 mm, respectively.

### 2.2. Silicalite zeolite membrane synthesis

Zeolite membranes were synthesized on the outer

surface of the porous mullite tubes. The molar gel compositions of the silicalite membranes were: 0.287-0.450 Na<sub>2</sub>O : 1.0 SiO<sub>2</sub> : 0.01-0.04 TPABr : 8-15 H<sub>2</sub>O, where TPABr was used as a template [18-23]. Sodium silicate and sodium aluminate were used as the Si and Al sources, respectively. For silicalite-1 preparation, two solutions were prepared; solution A: sodium silicate and solution B: TPABr + H<sub>2</sub>O + NaOH. Solution A was added to solution B with stirring. To obtain a homogeneous gel, the mixtures were stirred for 2 h at room temperature.

For membrane preparation, two ends of the supports were closed with rubber caps to avoid any precipitation of the zeolite crystals on the inner surface of the supports during membrane synthesis. The seeded supports were placed vertically in a Teflon autoclave. The solution was carefully poured into the autoclave and then the autoclave was sealed. Crystallization was carried out in an oven at a temperature 180 °C for 24 h. Then, the samples were taken and the synthesized membranes were washed several times with distilled water. The samples were then dried in air at room temperature for 12 h and then dried in the oven at 100 °C for 15 h to remove water occluded in the zeolite crystals and then calcinations were carried out in air at 530 °C for 8 h at a heating rate of 1 °C/min [21, 10, 23-28].

Phase identification was performed by XRD (Philips PW1710, Philips Co., Netherlands) with CuK $\alpha$  radiation. Also, morphological studies were performed using SEM (JEM-1200 or JEM-5600LV equipped with an Oxford ISIS-300 X-ray disperse spectroscopy, EDS).

### 2.3. Pervaporation tests

While the PV system was at steady state after 20 min, weight of permeate was measured at the 30 min period and then flux was calculated (surface area of the zeolite membrane was 44 cm<sup>2</sup>).

The zeolite membranes were used for long-term dehydration of UDMH aqueous solutions. Experiments were carried out at a temperature of 30 °C and a pressure of 1.5 mbar at the permeate side, within a period of 30-60 min.

The pervaporation setup is presented in Figure 1. Any change of feed concentration due to the permeation is negligible because the amount of permeate is small (max. 2 ml) compared to the total feed volume in the system (0.5 lit). A three stage diaphragm vacuum pump

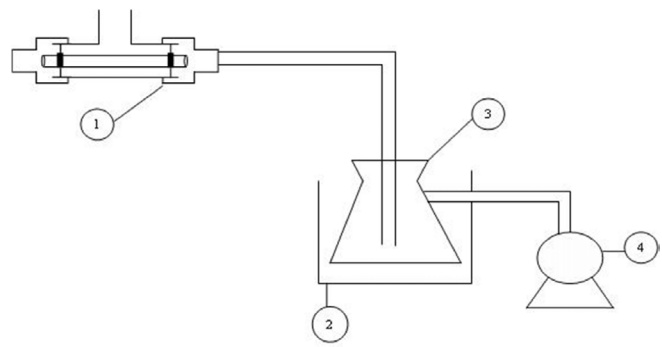


**Fig. 1.** PV setup; 1: feed container and PV cell, 2: liquid nitrogen trap, 3: permeate container, 4: three stage vacuum pump.

(vacuubrand, GMBH, Germany) was employed to evacuate the permeate side of the membrane to a pressure of approximately 1.5 mbar while the feed side was kept at room pressure. The permeate side was connected to a liquid nitrogen trap via a hose to condense the permeate (vapor). Permeate concentrations were measured using GC (TCD detector, Varian 3400, carrier gas: hydrogen, column: polyethylene glycol, sample size: 5  $\mu$ m, column and detector temperatures: 120-150 °C, detector flow: 15 ml/min, carrier flow: 5 ml/min, column pressure: 1.6 kPa, GC input pressure: 20 kPa). Performance of PV was evaluated using values of total flux (kg/m<sup>2</sup>.h) and separation factor (dimensionless). The separation factor of UDMH aqueous solution ( $\alpha$ ) can be calculated from the following equation:

$$\alpha = \frac{[y_{H_2O}/y_{UDMH}]}{[x_{H_2O}/x_{UDMH}]} \quad (2)$$

where  $y_{H_2O}$  and  $y_{UDMH}$  are the weight fractions of water and UDMH in the permeate, and  $x_{H_2O}$  and  $x_{UDMH}$  are weight fractions in the feed, respectively [29-31].

### 3. Modeling

Figure 2 represents the schematic diagram of the model domain used in the simulation. Feed solution containing a mixture of 5 wt% UDMH and 95 wt% water flows tangentially through the upper side of the membrane system ( $z=0$ ) and exits at  $z=L$ .

The main assumptions to develop the numerical simulation are as follows:

- Steady state condition is considered,
- Temperature is constant,
- No chemical reaction occurs in the feed stream,
- Feed solution flows only in the  $z$  direction,

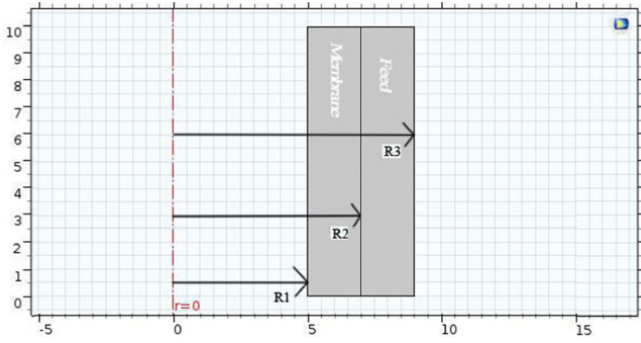


Fig. 2. Vertical diagram of the geometry of the model domain used in simulation

- Feed flow is laminar in the membrane system,
- Thermodynamic equilibrium is considered at the interface of the feed and membrane,
- A small amount of UDMH permeates through the membrane,
- Mass transfer resistance of the support layer is assumed to be negligible,
- Fouling and concentration polarization effects on the PV of UDMH solution are negligible and
- Feed viscosity and density are constant.

Axial and radial diffusions inside the membrane and feed phase are considered in the continuity equations. Moreover, small permeation of UDMH through the membrane is considered in the simulation by applying the selectivity equation (2).

Concentration of UDMH in the permeate side ( $y_{UDMH}$ ) must be determined by the trial and error method. In this method, an initial value for  $y_{UDMH}$  is guessed. Then the concentration the permeate side is calculated using model equations. This calculated value will then be compared with the guessed value. If the difference between the old and new values is less than a determined error, the guessed UDMH concentration is considered as the correct concentration. Otherwise, another guess must be made for  $y_{UDMH}$ .

Mass transport in the membrane system is described using the continuity equation. The following equation presents the differential form of this equation [32]:

$$\frac{\partial C_{H_2O}}{\partial t} + \nabla \cdot (-D_{H_2O} \nabla C_{H_2O} + U \cdot C_{H_2O}) = R \quad (3)$$

where  $C_{H_2O}$ ,  $D_{H_2O}$ ,  $U$  and  $R$  denote the water concentration ( $\text{mol}/\text{m}^3$ ), water diffusion coefficient ( $\text{m}^2/\text{s}$ ), velocity vector ( $\text{m}/\text{s}$ ) and reaction term ( $\text{mol}/\text{m}^3 \cdot \text{s}$ ), respectively. Since no chemical reactions take place in UDMH/water PV, the reaction term is zero. The continuity equation

was defined and solved in COMSOL Multiphysics 5.2 by adding a “transport of diluted species” physic to the whole model.

Velocity distribution was obtained by solving the Navier-Stokes equation for momentum balance, simultaneously with the continuity equation in the feed section. This was done by adding a “laminar flow” physic to the whole model in COMSOL Multiphysics 5.2. The following equation describes the momentum conservation equation [32]:

$$\rho \frac{\partial u}{\partial t} + \rho(u \cdot \nabla)u = \nabla \cdot [-P + \mu(\nabla u + (\nabla u)^T)] + F \quad (4)$$

$$\nabla \cdot (u) = 0 \quad (5)$$

where  $u$ ,  $\rho$ ,  $P$ ,  $\mu$  and  $F$  denote the z-component of the velocity vector ( $\text{m}/\text{s}$ ), feed density ( $\text{kg}/\text{m}^3$ ), pressure (Pa), feed viscosity (Pa.s) and body force (N), respectively.

### 3.1. Feed phase simulation

By applying the mentioned assumptions to Eq. (3), the steady state form of the continuity equation for water mass transport in the feed side is obtained:

$$-\frac{1}{r} \frac{\partial}{\partial r} \left( D_{H_2O} r \frac{\partial C_{H_2O-feed}}{\partial r} \right) - \frac{\partial}{\partial z} \left( D_{H_2O} \frac{\partial C_{H_2O-feed}}{\partial z} \right) + u \frac{\partial C_{H_2O-feed}}{\partial z} = 0 \quad (6)$$

where  $C_{H_2O-feed}$  is the water concentration in the feed phase. The simplified form of the momentum transport equations considering the above assumptions will be as follows:

$$\rho \left( u \frac{\partial u}{\partial z} \right) - \frac{1}{r} \frac{\partial}{\partial r} \left( r \mu \frac{\partial u}{\partial r} \right) - \frac{\partial}{\partial z} \left( \mu \frac{\partial u}{\partial z} \right) = -\frac{\partial P}{\partial z} \quad (7)$$

$$\frac{\partial u}{\partial z} = 0 \quad (8)$$

where  $r$  and  $z$  denote the radial and axial coordinates, respectively.

The initial conditions for mass and momentum conservation equations are as follows:

$$C_{H_2O-feed} = C_{0,H_2O} \quad \text{and} \quad u = u_0 \quad (9)$$

where  $C_{0,H_2O}$  is the water initial concentration and  $u_0$  is the initial velocity of the feed flow.

The boundary conditions for mass conservation

equations in the feed phase are as follows:

$$\text{at } z = L, \text{ Outflow condition} \quad (10)$$

$$\text{at } z = 0, C_{H_2O-feed} = C_{0,H_2O} \quad (11)$$

$$\text{at } r = R_3, \text{ No flux condition} \quad (12)$$

where  $R_3$  is the outer radius of the feed section. At the interface of the membrane-feed, the equilibrium condition is assumed:

$$\text{at } r = R_2, C_{H_2O-feed} = \frac{C_{H_2O-membrane}}{p} \quad (13)$$

in which  $C_{H_2O-membrane}$  is the water concentration in the membrane section and  $p$  is the partition coefficient obtained from the selectivity equation as follows:

$$p = \frac{y_{UDMH}}{x_{UDMH}} \times \alpha = \frac{y_{H_2O}}{x_{H_2O}} \quad (14)$$

As mentioned earlier, the permeate concentration of UDMH must be determined using the trial and error method, and then is placed in the above equation.

The boundary conditions for momentum transfer equations are as follows:

$$\text{at } z = 0, u = u_0, \text{ (Inlet velocity)} \quad (15)$$

At the outlet, the pressure is atmospheric pressure:

$$\text{at } z = L, P = P_{atm}, \text{ (Atmospheric pressure)} \quad (16)$$

$$\text{at } r = R_2, u = 0 \text{ (No slip condition)} \quad (17)$$

$$\text{at } r = R_3, u = 0 \text{ (No slip condition)} \quad (18)$$

### 3.2. Membrane phase simulation

Mass transport of water in the membrane is controlled only by the diffusion mechanism. Therefore, the steady state continuity equation for water can be written as:

$$-\frac{1}{r} \frac{\partial}{\partial r} \left( D_{H_2O-membrane} r \frac{\partial C_{H_2O-membrane}}{\partial r} \right) - \frac{\partial}{\partial z} \left( D_{H_2O-membrane} \frac{\partial C_{H_2O-membrane}}{\partial z} \right) = 0 \quad (19)$$

where  $D_{H_2O-membrane}$  is the water diffusion coefficient in the membrane ( $m^2/s$ ).

Membrane phase boundary conditions are given as:

$$\text{at } r = R_2, C_{H_2O-membrane} = p \times C_{H_2O-feed} \text{ (Equilibrium condition)} \quad (20)$$

$$\text{at } r = R_1, C_{H_2O-membrane} = 0 \text{ (Dry membrane condition)} \quad (21)$$

$$\text{at } z = 0 \text{ and } z = L, \frac{\partial C_{H_2O-membrane}}{\partial z} = 0 \text{ (No flux condition)} \quad (22)$$

At the permeate-membrane interface, water concentration was assumed to be zero due to the vacuum applied.

### 3.3. Numerical solution of conservation equations

The set of model equations, including mass and momentum transfer equations in the membrane module along with suitable boundary conditions, was solved using COMSOL Multiphysics software version 5.2. Finite element method is used by this software to solve conservation equations numerically. The computational time for solving the equations was about 2 min. ‘‘Extra fine mesh’’ was used for meshing in this simulation. Complete mesh consisted of 30558 domain elements and 975 boundary elements to solve the set of equations. Figure 3 represents the meshes created by COMSOL Multiphysics 5.2 software. Due to the considerable difference between  $z$  and  $r$  dimensions, a scaling factor equal to 10 was used in the  $z$  direction. Therefore, the results were reported in dimensionless length.

## 4. Results and discussion

It is well known that PV performance of a dense polymeric membrane depends on the ability of solvent

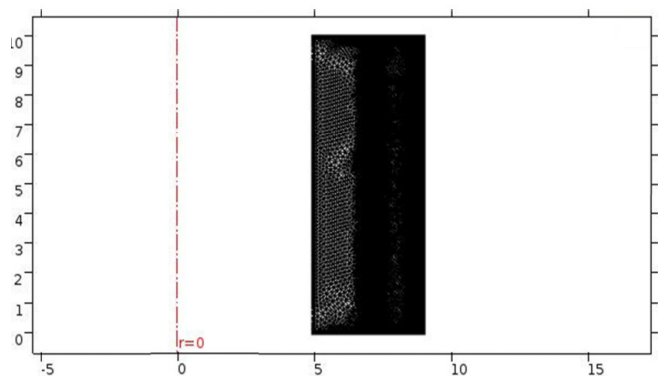


**Fig. 3.** Meshes created by COMSOL Multiphysics 5.2; Complete mesh consisted of 30558 domain elements.

species to be dissolved in the membrane at its interfaces, and their diffusion into the membrane. When a zeolite membrane is used as a separation barrier the solvent species cannot be dissolved in the membrane phase, but they are adsorbed on the zeolite sites of the inorganic materials. Their adsorbed capacities depend on the affinity of the membranes towards the solvents to be removed.

#### 4.1. Silicalite-1 performance

The membrane exhibited a high selectivity towards water in water–UDMH mixtures. The permeate water flux reached a value as high as 3.34 kg/m<sup>2</sup>.h for a UDMH concentration of 5 wt%. The fact that the membrane has a high selectivity towards water clearly indicates that the zeolite layer does not have any through-holes, and the transport is diffusive but not convective.

Silicalite-1 membrane showed a water-UDMH ideal selectivity of 10000 at 27°C, indicating its reasonable quality. During PV, water permeates through both zeolite and non-zeolite pores because of its small diameter. The kinetic diameter of UDMH is larger than the diameter of zeolite pores, thus much of the UDMH flux probably passes through the non-zeolite pores. Since the silicalite-1 is a weak hydrophilic membrane, the water flux decreases. The diffusing molecules in these mixtures pass via viscous flow and molecular sieve; whereas, viscous flow requires a pressure gradient across the membrane. If the zeolite is defect-free it has no non-zeolite pores, and thus water can pass only through zeolite pores (Table 2). However, non-zeolite pores usually exist and are larger than the zeolite pores. Non-zeolite pores have a size distribution and may also affect flux and selectivity. Transport through non-zeolite pores has contributions from both surface diffusion and Knudsen diffusion, and possibly from viscous flow.

The Silicalite channel system is shown in Figure 4. The straight elliptical channels running in the b-direction have dimensions of 0.53×0.56 nm, and the sinusoidal

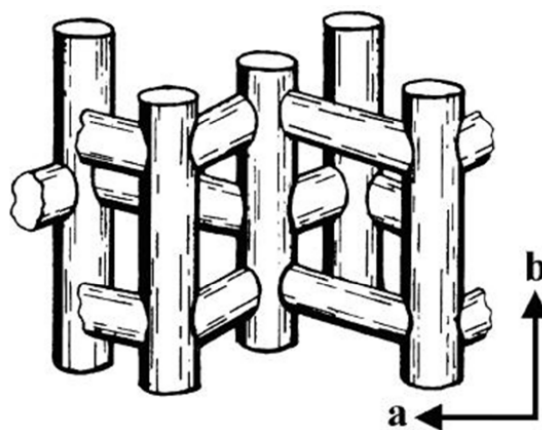


Fig. 4. Silicalite channel system.

channels running in the a-direction have dimensions of 0.55×0.51 nm.

Figure 5 shows XRD patterns of the mullite support and the zeolite membranes. Morphology of the support subjected to crystallization was characterized by SEM (Figure 6). Figure 7 shows the morphology of the silicalite-1 membranes (surface and cross section). As seen, most of the crystals lie disorderly on the surface. The SEM photographs of the membranes (cross section) show that the mullite surface is completely covered by a zeolite crystal layer, whose thickness is larger than 40 μm. The crystal layer is composed of two layers; the top layer consists of pure Silicalite crystals and the intermediate one of Silicalite crystals grown into the mullite pores.

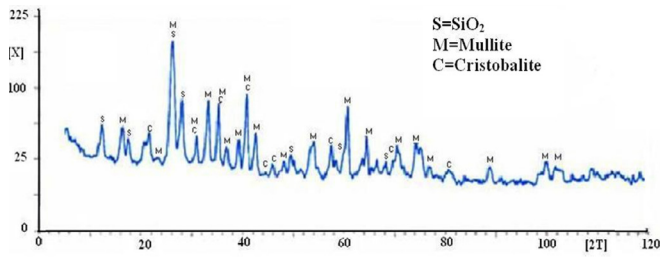
As seen in Table 2, the best selectivity for silicalite-1 was 53% and the best water flux was 3.34 kg/m<sup>2</sup>.h at 27°C. The best silicalite-1 membranes were prepared using the following gel molar composition: 0.287 Na<sub>2</sub>O:1.0 SiO<sub>2</sub>:0.04 TPABr: 15 H<sub>2</sub>O.

#### 4.2. Feed phase simulations

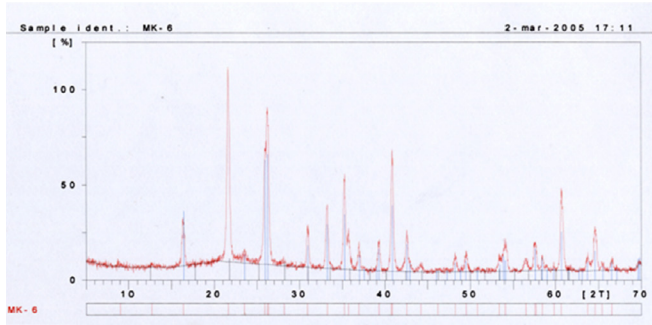
Figure 8 shows the surface concentration distribution of water in half of the feed section at steady state conditions. The UDMH/water solution containing 95 wt% water flows over the outer surface of the membrane

Table 2. Flux and separation factor of the silicalite zeolite membranes.

Sample	Na <sub>2</sub> O/SiO <sub>2</sub>	TPABr/SiO <sub>2</sub>	H <sub>2</sub> O/SiO <sub>2</sub>	T (°C)	t (h)	UDMH (%)	Flux (kg/m <sup>2</sup> .h)	Separation factor
1	0.450	0.01	8	180	24	5	1.02	4
2	0.287	0.01	8	180	24	5	1.67	8
3	0.350	0.01	8	180	24	5	1.7	23
4	0.350	0.04	15	180	24	5	3.34	53



(a) Support



(b) Silicalite

**Fig. 5.** XRD patterns of the (a) support and (b) silicalite zeolite membrane.

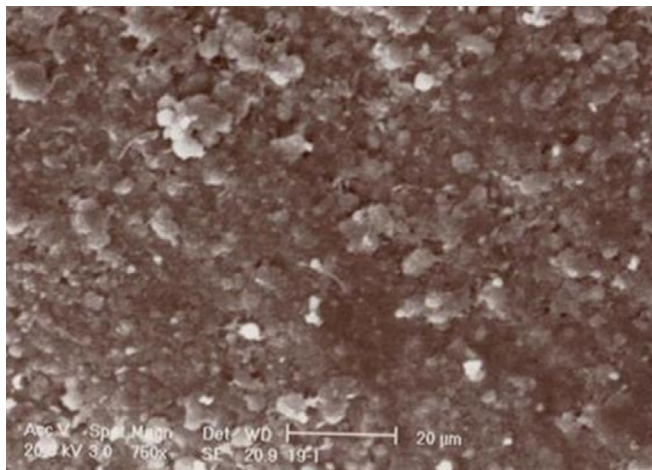
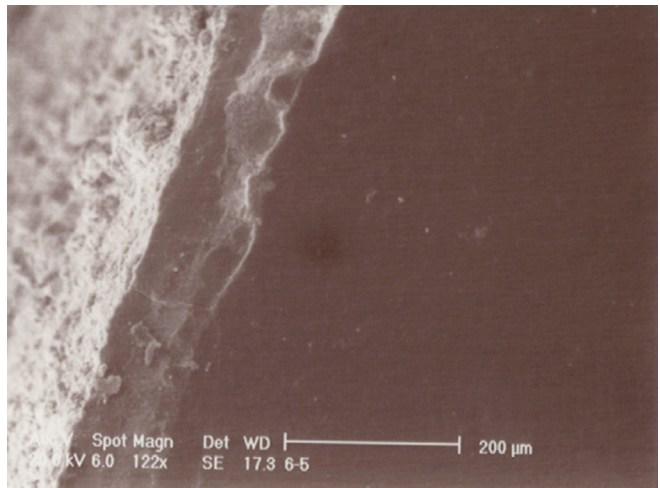
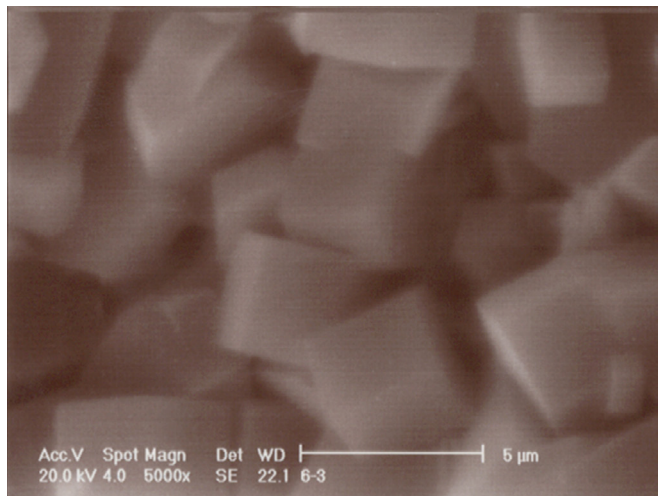


**Fig. 6.** SEM micrograph of the support.

module ( $z=0$ ). As can be seen from the figure 8, a concentration boundary layer is formed on the membrane-feed interface. At  $z=0$ , the water concentration is maximum (95 wt%). As the feed solution flows in the feed compartment, water moves towards the membrane surface due to the concentration and pressure differences (driving forces). Therefore, the water concentration on the membrane surface is less than its value at the feed inlet (where water concentration is equal to its initial value,  $C_{0, H_2O - feed}$ ). The water accumulation on the membrane surface was calculated from the membrane selectivity (Eq. 13) and its value in on the membrane side. Since water concentration in the membrane is always less than its value in the feed, the



(a) Surface



(b) Cross section

**Fig. 7.** SEM of the silicalite zeolite membrane; (a) surface and (b) cross section

water concentration on the membrane-feed boundary ( $r=R_2$ ) is always less than its value in the feed bulk.

Figure 9 presents the water distribution in the feed phase versus the  $r$ -coordinate at different lengths. Water concentration increases along the  $r$  direction, as expected. The concentration gradient is great at regions

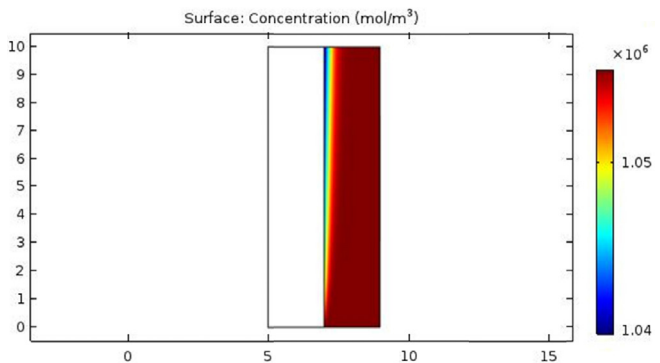


**Fig. 8.** Surface concentration distribution of water in feed phase (1.5 l/min feed flow rate and 30 °C temperature).

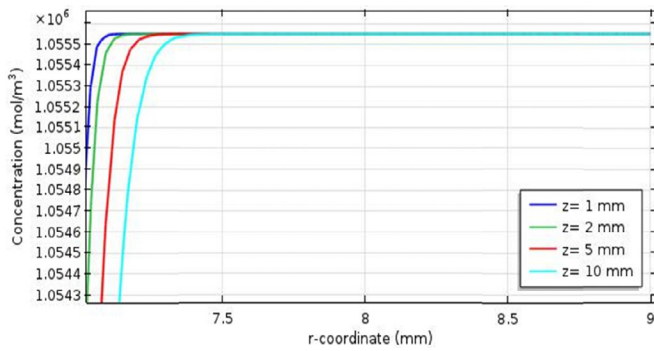
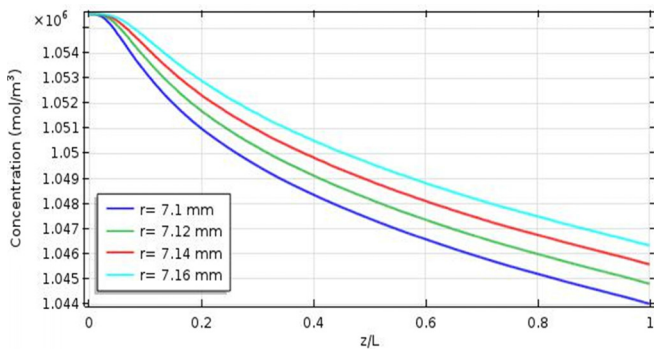


**Fig. 9.** Concentration distribution of water in feed phase vs. radius at various membrane lengths (1.5 l/min feed flow rate and 30 °C temperature).

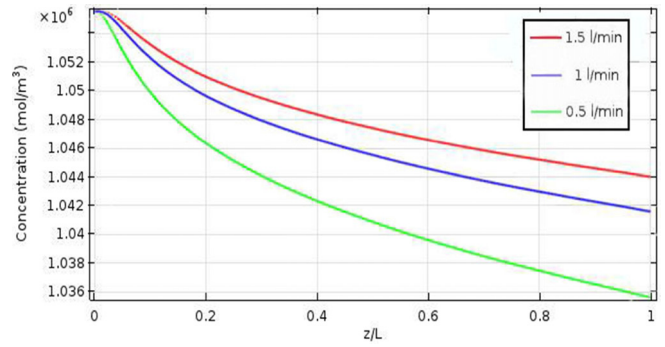
near the membrane-feed interface ( $r=R_2$ ) due to the mass transfer towards the membrane at this region.

Figure 10 demonstrates the concentration distribution along the z coordinate at a constant flow rate (1.5 l/min) and different radii. Results indicate that the variation of water concentration along the z coordinate is considerable and cannot be neglected compared to its variation along the r coordinate. The figure also shows that the concentration gradient near the membrane-feed interface ( $r=7.1$  mm) is slightly greater, while it is less at greater radii. This behavior can be attributed to water transfer towards the membrane at this region (greater concentration gradients).

Figure 11 shows the effect of various feed flow rates on water concentration distribution within the feed section. As can be seen, water concentration increases with increasing feed flow rate. This is because higher velocities (or flow rates) would decrease the contact time of the feed flow with the membrane, thus less water has enough time to pass through the membrane. Therefore, much higher concentrations will be obtained at higher feed flow rates.



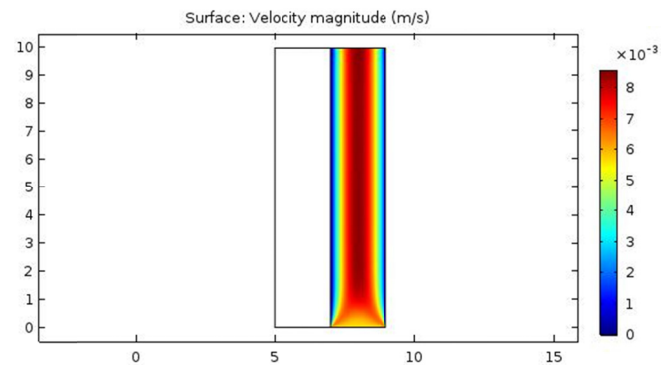
**Fig. 10.** Water concentration distribution in feed phase vs. dimensionless length (1.5 l/min feed flow rate and 30 °C temperature) at various radii.



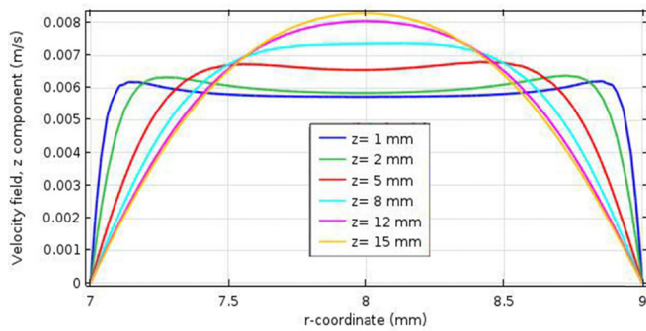
**Fig. 11.** Water concentration in feed section at different feed flow rates (at 30 °C temperature).

Figure 12 shows the velocity field in the feed phase of the PV membrane system. The velocity distribution was obtained using numerical solution of momentum balance. This was done by adding a “laminar flow” physic to the whole model in COMSOL. As can be seen from the figure, the velocity profile is fully developed after a short distance. Velocity is zero on the membrane-feed interface and outer boundary of the feed section due to the no slip condition.

Figure 13 shows the velocity profile vs. radius in the feed section. As can be seen, the velocity profile is parabolic and becomes fully developed after a short distance (lengths approximately more than 12 mm). As seen, entrance effects are considered in this simulation, which is one of the advantages of FEM simulation. Figure 14 represents velocity distribution vs. dimensionless length at different feed flow rates. The velocity profile is almost parabolic and reaches its maximum value at the regions close to the feed entrance. Maximum velocity magnitude increases with increasing feed flow rate.



**Fig. 12.** Velocity distribution in the feed phase at 1.5 l/min feed flow rate and 30 °C temperature.



**Fig. 13.** Velocity profile vs. r-coordinate at various membrane lengths (1.5 l/min feed flow rate and 30 °C temperature).

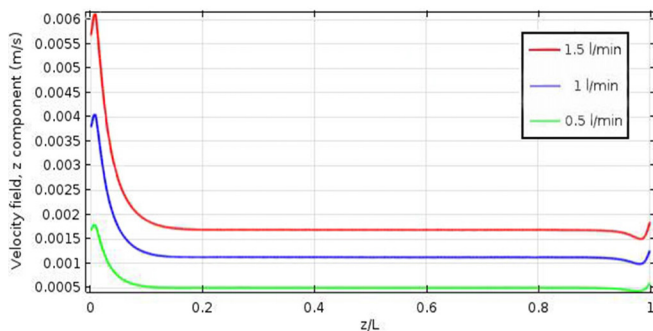


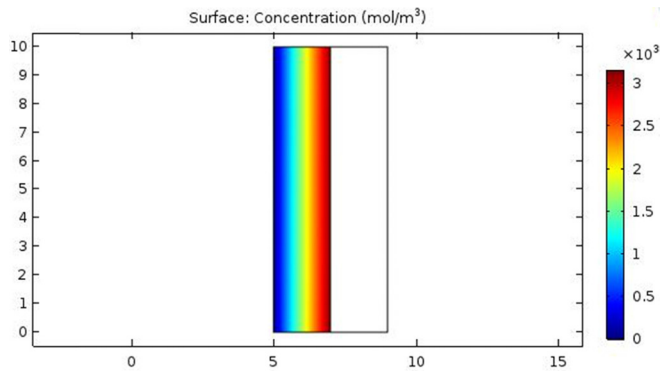
**Fig. 14.** Velocity profile vs. dimensionless length at different feed flow rates.

#### 4.3. Membrane phase simulation

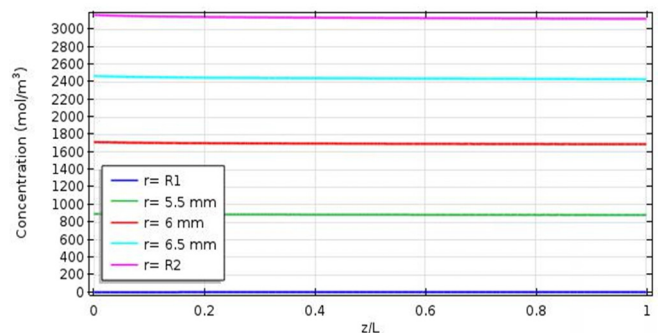
Figure 15 shows the concentration distribution of water in the membrane phase at steady state conditions. The water transfer mechanism through the membrane was described only by diffusion. Since vacuum condition was assumed at the membrane-permeate interface, the water concentration on this boundary is zero. Water concentration is highest on the membrane-feed interface because it is calculated from its value in the feed section, which is always highest.

Figure 16 demonstrates water concentration distribution within the membrane vs. dimensionless length at a constant flow rate (1.5 l/min) and different membrane radii. Results show that the variation of water concentration along the z coordinate at constant radius is not considerable and can be neglected.

Figure 17 shows the effect of various feed flow rates on water concentration distribution within the membrane. As can be seen from the figure, water concentration increases with increasing feed flow rate. This is because an increase in feed flow rate would result in much higher concentrations in the feed compartment. Since water concentration in the membrane is calculated from its value on the feed side, much more water concentrations in the membrane will be obtained at higher feed flow rates.



**Fig. 15.** Concentration distribution of water in membrane phase at 1.5 l/min feed flow rate and 30 °C temperature.



**Fig. 16.** Concentration distribution of water in membrane phase vs. dimensionless length at different radii (1.5 l/min feed flow rate and 30 °C temperature).

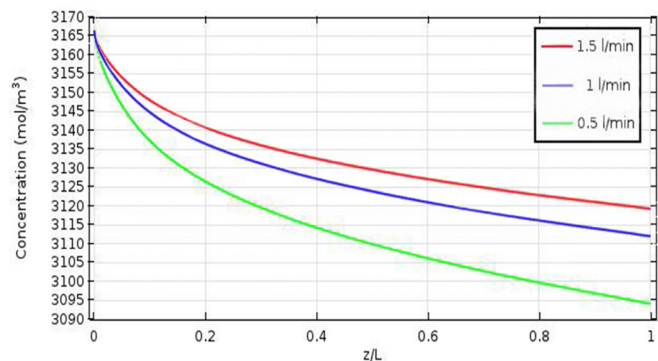


**Fig. 17.** Water concentration profile vs. dimensionless length at different feed flow rates (30 °C temperature).

## 5. Conclusion

Silicalite zeolite membranes were first used for dehydration of water-UDMH mixtures. The membranes were synthesized on the outer surface of porous mullite tubes by the hydrothermal method. The mullite supports were made by extruding kaolin clay. The zeolite membranes showed much higher fluxes and separation factors than commercially available polymeric membranes. The membranes showed good membrane performance for separation of the UDMH-

mixtures. It is expected that even significantly higher fluxes, with similar separation factors, can be achieved at higher temperatures. Performance of PV system was modeled using COMSOL Multiphysics software version 5.2. Modeling was conducted by solving mass and momentum equations numerically using the finite element method (FEM). Good modeling results indicated that FEM is a powerful method for simulating membrane separation systems.

Since the silicalite zeolite membranes can withstand high temperatures and harsh environments ( $\text{pH} > 12$ ), dehydration of the water-UDMH mixtures can be performed. It was found that PV using the Silicalite zeolite membranes is an effective technique to separate water from the water-UDMH mixtures.

### Nomenclature

$C_{0,H_2O}$	initial water concentration ( $\text{mol}/\text{m}^3$ )
$C_{H_2O}$	water concentration ( $\text{mol}/\text{m}^3$ )
$C_{H_2O - \text{feed}}$	water concentration in feed phase ( $\text{mol}/\text{m}^3$ )
$C_{H_2O - \text{membrane}}$	water concentration in membrane phase ( $\text{mol}/\text{m}^3$ )
$D_{H_2O}$	water diffusion coefficient ( $\text{m}^2/\text{s}$ )
$D_{H_2O - \text{membrane}}$	water diffusion coefficient in membrane ( $\text{m}^2/\text{s}$ )
F	body force (N)
L	membrane length (mm)
p	partition coefficient
P	pressure (Pa)
$P_{\text{atm}}$	atmospheric pressure (Pa)
r	radial coordinate
$R_1$	permeate-membrane radius (mm)
$R_2$	membrane-feed radius (mm)
$R_3$	Outer radius of the feed section (mm)
R	reaction term ( $\text{mol}/\text{m}^3 \cdot \text{s}$ )
$\alpha$	selectivity
t	separation time (s)
U	velocity vector (m/s)
u	z-component velocity (m/s)
$x_{UDMH}$	UDMH wt% in feed
$x_{H_2O}$	water wt% in feed
$y_{UDMH}$	UDMH wt% in permeate
$y_{H_2O}$	water wt% in permeate
z	axial coordinate
$\rho$	density ( $\text{kg}/\text{m}^3$ )
$\mu$	viscosity (Pa.s)

### References

- [1] R. Ravindra K.R. Krovvidi, A.A. Khan, A.K. Rao, D.S.C. studies of states of water, hydrazine and hydrazine hydrate in ethyl cellulose membrane, *Polymer*, 40 (1999) 1159-1165.
- [2] R. Ravindra, A. Kameswara, A. Khan, A qualitative evaluation of water and monomethyl hydrazine in ethyl cellulose membrane, *J. Appl. Polym. Sci.* 72 (1999) 689-700.
- [3] S. Sridhar, G. Susheela, G.J. Reddy, A.A. Khan, Cross linked chitosan membranes: characterization and study of dimethylhydrazine dehydration by pervaporation, *Polym. Int.* 50 (2001) 1156-1165.
- [4] S. Moulik, K.P. Kumar, S. Bohra, S. Sridhar, Pervaporation performance of PPO membranes in dehydration of highly hazardous MMH and UDMH liquid propellants, *J. Hazard. Mater.* 288 (2015) 69-79.
- [5] Y-L. Liao, C-C. Hu, J-Y. Lai, Y-L. Liu, Cross-linked polybenzoxazine based membrane exhibiting in-situ self-promoted separation performance for pervaporation dehydration on isopropanol aqueous solutions, *J. Membrane Sci.* 531 (2017) 10-15.
- [6] Y.M. Xu, T-S. Chung, High-performance UiO-66/polymide mixed matrix membranes for ethanol, isopropanol and n-butanol dehydration via pervaporation, *J. Membrane Sci.* 531 (2017) 16-26.
- [7] S. Zhang, Y. Zou, T. Wei, C. Mu, X. Liu, Z. Tong, Pervaporation dehydration of binary and ternary mixtures of n-butyl acetate, n-butanol and water using PVA-CS blended membranes, *Sep. Purif. Technol.* 173 (2017) 314-322.
- [8] J. Liu, R. Bernstein, High-flux thin-film composite polyelectrolyte hydrogel membranes for ethanol dehydration by pervaporation, *J. Membrane Sci.* 534 (2017) 83-91.
- [9] T. Uragami, M. Banno, T. Miyata, Dehydration of an ethanol/water azeotrope through alginate-DNA membranes cross-linked with metal ions by pervaporation, *Carbohydr. Polym.* 134 (2015) 38-45.
- [10] D.A. Fedosov, A.V. Smirnov, V.V. Shkirskiy, T. Voskoboinikov, I.I. Ivanova, Methanol dehydration in NaA zeolite membrane reactor, *J. Membrane Sci.* 486 (2015) 189-194.
- [11] R. Ravindra, S. Sridhar, A.A. Khan, A.K. Rao, Pervaporation of water, hydrazine and monomethylhydrazine using ethyl cellulose membranes, *Polymer*, 41 (2000) 2795-2806.

- [12] S. Sridhar, R. Ravindra, A.A. Khan, Recovery of monomethylhydrazine liquid propellant by pervaporation technique, *Ind. Eng. Chem. Res.* 39 (2001) 2485-2490.
- [13] X. Li, I. Kresse, Z.K. Zhou, J. Springer, Effect of temperature and pressure on gas transport in ethyl cellulose membrane, *Polymer*, 42 (2001) 6801-6810.
- [14] Y-H. Huang, Q-F. An, T. Liu, W-S. Hung, C-L. Li, S-H. Huang, C-C. Hu, K-R. Lee, J-Y. Lai, Molecular dynamics simulation and positron annihilation lifetime spectroscopy: Pervaporation dehydration process using polyelectrolyte complex membranes, *J. Membrane Sci.* 451 (2014) 67-73.
- [15] M. Jain, D. Attarde, S.K. Gupta, Removal of thiophenes from FCC gasoline by using a hollow fiber pervaporation module: Modeling, validation and influence of module dimensions and flow directions, *Chem. Eng. J.* 308 (2017) 632-648.
- [16] S. Moulik, S. Nazia, B. Vani, S. Sridhar, Pervaporation separation of acetic acid/water mixtures through sodium alginate/polyaniline polyion complex membrane, *Sep. Purif. Technol.* 170 (2016) 30-39.
- [17] N.S. Prasad, S. Moulik, S. Bohra, K.Y. Rani, S. Sridhar, Solvent resistant chitosan / poly(ether-block-amide) composite membranes for pervaporation of n-methyl-2-pyrrolidone / water mixtures, *Carbohydr. Polym.* 136 (2016) 1170-1181.
- [18] M. Kazemimoghadam, A. Pak, T. Mohammadi, Dehydration of water / 1-1-dimethylhydrazine mixtures by zeolite membranes, *Micropor. Mesopor. Mat.* 70 (2004) 127-134.
- [19] L. Zhoua, T. Wang, Q.T. Nguyenc, J. Li, Y. Long, Z. Ping, Cordierite-supported ZSM-5 membrane: Preparation and pervaporation properties in the dehydration of water-alcohol mixture, *Sep. Purif. Technol.* 44 (2005) 266-270.
- [20] F. Akhtar, E. Sjöberg, D. Korelskiy, M. Rayson, J. Hedlund, L. Bergström, Preparation of graded silicalite-1 substrates for all-zeolite membranes with excellent CO<sub>2</sub>/H<sub>2</sub> separation performance, *J. Membrane Sci.* 493 (2015) 206-211.
- [21] G. Li, E. Kikuchi, M. Matsukata, A study on the pervaporation of water-acetic acid mixtures through ZSM-5 zeolite membranes, *J. Membrane Sci.* 218 (2003) 185-194.
- [22] J. LP, Q.T. Nguyen, L.Z. Zhou, T. Wang, Y.C. Long, Z.H. Ping, Preparation and properties of ZSM-5 zeolite membrane obtained by low-temperature chemical vapor deposition, *Desalination*, 147 (2002) 321-326.
- [23] T. Masuda, S-H Otani, T. Tsuji, M. Kitamura, S.R. Mukai, Preparation of hydrophilic and acid-proof silicalite-1 zeolite membrane and its application to selective separation of water from water solutions of concentrated acetic acid by pervaporation, *Sep. Purif. Technol.* 32 (2003) 181-189.
- [24] B. Oonkhanond, M.E. Mullins, The preparation and analysis of zeolite ZSM-5 membranes on porous alumina supports, *J. Membrane Sci.* 194 (2001) 3-13.
- [25] M. Nomura, T. Yamaguchi, S-I Nakao, Transport phenomena through intercrystalline and intracrystalline pathways of silicalite zeolite membranes, *J. Membrane Sci.* 187 (2001) 203-212.
- [26] M. A. Baig, F. Patel, K. Alhooshani, O. Muraza, E.N. Wang, T. Laoui, In-situ aging microwave heating synthesis of LTA zeolite layer on mesoporous TiO<sub>2</sub> coated porous alumina support, *J. Cryst. Growth*, 432 (2015) 123-128.
- [27] T.C. Bowen, R.D. Noble, J.L. Falconer, Fundamentals and applications of pervaporation through zeolite membranes, *J. Membrane Sci.* 245 (2004) 1-33.
- [28] C. Algieri, P. Bernardo, G. Golemme, G. Barbieri, E. Drioli, Permeation properties of a thin silicalite-1 (MFI) membrane, *J. Membrane Sci.* 222 (2003) 181-190.
- [29] M. Nomura, T. Bin, S-I Nakao, Selective ethanol extraction from fermentation broth using a silicalite membrane, *Sep. Purif. Technol.* 27 (2002) 59-66.
- [30] S. Nai, X. Liu, W. Liu, B. Zhang, Ethanol recovery from its dilute aqueous solution using Fe-ZSM-5 membranes: Effect of defect size and surface hydrophobicity, *Micropor. Mesopor. Mat.* 215 (2015) 46-50.
- [31] A.M. Avila, Z. Yu, S. Fazli, J.A. Sawada, S.M. Kuznicki, Hydrogen-selective natural mordenite in a membrane reactor for ethane dehydrogenation, *Micropor. Mesopor. Mat.* 190 (2014) 301-308.
- [32] R.B. Bird, W.E. Stewart, E.N. Lightfoot, *Transport Phenomena*, 2<sup>nd</sup> edition, John Wiley & Sons, New York, 1960, pp. 780.